

Direct detection of pseudo-Nambu-Goldstone dark matter with light mediator

Yoshihiko Abe^{1*} and Takashi Toma^{2,3†}

¹*Department of Physics, Kyoto University, Kyoto 606-8502, Japan*

²*Institute of Liberal Arts and Science, Kanazawa University, Kanazawa, 920-1192 Japan*

³*Institute for Theoretical Physics, Kanazawa University, Kanazawa 920-1192, Japan*

Abstract

It has been found that a pseudo-Nambu-Goldstone boson dark matter suppresses the amplitude for elastic scattering with nuclei in non-relativistic limit, and thus can naturally evade the strong constraint of dark matter direct detection experiments. In this paper, we show that non-zero elastic scattering cross section can be induced if the mediator mass is as small as momentum transfer. The predicted recoil energy spectrum can differ from that for usual thermal dark matter. Together with the relevant constraints such as thermal relic abundance, indirect detection and Higgs decays, we investigate the detectability through the current and future dark matter direct detection experiments.

*y.abe@gauge.scphys.kyoto-u.ac.jp

†toma@staff.kanazawa-u.ac.jp

1 Introduction

Dark matter direct detection experiments impose strong bounds on thermal dark matter. The current strongest bound is given by the XENON1T/PandaX-4T [1,2], and will be further updated by the future XENONnT experiment [3]. The pseudo-Nambu-Goldstone boson (pNGB) dark matter has been proposed as a candidate naturally evading this strong constraint [4]. This is because the amplitude of the elastic scattering with nuclei is suppressed by the small momentum of dark matter through the derivative coupling. A non-zero elastic cross section is induced at loop levels, however it is marginally small compared to future sensitivities [5–7]. In addition, a sophisticated global fit of the model with relevant constraints has also been performed [8].

For the pNGB dark matter model, an explicit soft breaking term is required to give a mass for the NGB after the spontaneous breaking of the corresponding global symmetry. It may be natural that the scale of the soft breaking term is much smaller than the scale of the spontaneous symmetry breaking in the sense that the global symmetry is approximate. However this is not necessarily true if a ultra-violet (UV) completion of the pNGB model is considered [9–12]. In this case, the effective pNGB model derived at low energy can have a soft breaking term larger than the scale of the spontaneous symmetry breaking. As a result, the mass of the particle mediating between dark matter and Standard Model (SM) particles can be much lighter than the dark matter mass.

In this paper, we consider the pNGB dark matter with a light mediator. In this scenario, we will show that non-zero elastic scattering cross section between dark matter and nuclei emerges even though the interactions arise from the derivative coupling. Furthermore, this scenario has a potential to discriminate the pNGB dark matter and the other dark matter candidates such as Weakly Interacting Massive Particles (WIMPs) by comparing the recoil energy spectrum of the event rate at direct detection. We contemplate some relevant constraints such as thermal production of dark matter, indirect detection bounds and Higgs invisible decay. Then, we show that some parameter region has already been excluded by the XENON1T bound, and some other region will be explored by the future XENONnT experiment.

2 The model

We consider the model extended with a complex singlet scalar S . The model has a global $U(1)_S$ symmetry under the transformation $S \rightarrow e^{i\alpha}S$, which is broken to the \mathbb{Z}_2 parity by introducing the soft breaking term S^2 . The soft breaking term can be derived from a UV completion of the model [9–12]. The Lagrangian is given by

$$\mathcal{L} = |\partial_\mu S|^2 - \mathcal{V}(H, S), \quad (2.1)$$

where the scalar potential \mathcal{V} is written down as

$$\mathcal{V} = -\frac{\mu_H^2}{2}|H|^2 - \frac{\mu_S^2}{2}|S|^2 + \frac{\lambda_H}{2}|H|^4 + \lambda_{HS}|H|^2|S|^2 + \frac{\lambda_S}{2}|S|^4 - \frac{m_\chi^2}{4}(S^2 + S^{*2}). \quad (2.2)$$

The λ_{HS} term is the Higgs portal coupling giving the interaction between the SM and S . The last term is the soft breaking term giving the mass to the NGB after the spontaneous symmetry breaking. Then, the scalar fields H and S can be parametrized as

$$H = \frac{1}{\sqrt{2}} \begin{pmatrix} 0 \\ v+h \end{pmatrix}, \quad S = \frac{1}{\sqrt{2}}(v_s + s) e^{i\chi/v_s}, \quad (2.3)$$

where $v, v_s \in \mathbb{R}$ are the vacuum expectation values for H and S , respectively. Because of the interests in the low energy dynamics of pNGB and the simplicity of calculation, we use the non-linear representation for S in this paper. These expectation values satisfy the following stationary conditions:

$$\mu_H^2 = \lambda_H v^2 + \lambda_{HS} v_s^2, \quad \mu_S^2 + m_\chi^2 = \lambda_S v_s^2 + \lambda_{HS} v^2. \quad (2.4)$$

The CP-even components h and s mix with each other via the Higgs portal coupling, and the mass matrix is given by

$$\begin{pmatrix} \lambda_H v^2 & \lambda_{HS} v v_s \\ \lambda_{HS} v v_s & \lambda_S v_s^2 \end{pmatrix}. \quad (2.5)$$

This mass matrix is diagonalized by the unitary matrix, and thus the gauge eigenstates h and s can be rewritten by the mass eigenstates h_1 and h_2 as

$$\begin{pmatrix} h \\ s \end{pmatrix} = \begin{pmatrix} \cos \theta & \sin \theta \\ -\sin \theta & \cos \theta \end{pmatrix} \begin{pmatrix} h_1 \\ h_2 \end{pmatrix}, \quad (2.6)$$

where h_1 is identified as the SM-like Higgs boson with the mass $m_{h_1} = 125$ GeV and h_2 is the second Higgs boson whose mass is assumed to be much lighter than m_{h_1} . The CP-odd component χ is the pNGB with the mass m_χ and can be a stable dark matter candidate due to a \mathbb{Z}_2 parity associated with the CP symmetry in the dark sector. The dark matter mass is given by the soft breaking parameter m_χ .

The quartic couplings λ_H , λ_{HS} and λ_S in the scalar potential can be rewritten in terms of the physical quantities as

$$\lambda_H = \frac{\cos^2 \theta m_{h_1}^2 + \sin^2 \theta m_{h_2}^2}{v^2}, \quad (2.7)$$

$$\lambda_{HS} = \frac{\sin \theta \cos \theta (m_{h_2}^2 - m_{h_1}^2)}{v v_s}, \quad (2.8)$$

$$\lambda_S = \frac{\sin^2 \theta m_{h_1}^2 + \cos^2 \theta m_{h_2}^2}{v_s^2}, \quad (2.9)$$

and the cubic couplings which are relevant to the subsequent sections are given by

$$\kappa_{111} = 3m_{h_1}^2 \left(-\frac{\sin^3 \theta}{v_s} + \frac{\cos^3 \theta}{v} \right), \quad (2.10)$$

$$\kappa_{112} = (2m_{h_1}^2 + m_{h_2}^2) \sin \theta \cos \theta \left(\frac{\sin \theta}{v_s} + \frac{\cos \theta}{v} \right), \quad (2.11)$$

$$\kappa_{122} = (m_{h_1}^2 + 2m_{h_2}^2) \sin \theta \cos \theta \left(-\frac{\cos \theta}{v_s} + \frac{\sin \theta}{v} \right), \quad (2.12)$$

$$\kappa_{222} = 3m_{h_2}^2 \left(\frac{\cos^3 \theta}{v_s} + \frac{\sin^3 \theta}{v} \right), \quad (2.13)$$

with the convention

$$\mathcal{V} \supset \frac{\kappa_{111}}{3!} h_1^3 + \frac{\kappa_{112}}{2!} h_1^2 h_2 + \frac{\kappa_{122}}{2!} h_1 h_2^2 + \frac{\kappa_{222}}{3!} h_2^3. \quad (2.14)$$

Note that the interactions between the dark matter and the SM particles come from the kinetic term $|\partial_\mu S|^2$ and the soft breaking term $-\frac{m_\chi^2}{4}(S^2 + S^{*2})$ since the field S is written in non-linear representation as Eq. (2.3).

It could be natural from the 't Hooft sense that the soft breaking parameter m_χ is much smaller than the scale of the spontaneous symmetry breaking v_s because the \mathbb{Z}_2 parity is enhanced to the global $U(1)_S$ symmetry in $m_\chi \rightarrow 0$ limit. However note that m_χ and v_s are irrelevant and can be regarded as independent parameters once a UV completion of the model is considered [9–12]. Therefore, in the following we consider the case of $v_s, m_{h_2} \ll m_\chi$. From Eq. (2.4) and $m_{h_2}^2 \approx \lambda_S v_s^2$, it is found that the quadratic mass parameter μ_S^2 should be negative and m_χ^2 is the trigger of the symmetry breaking in this case. Although the breaking pattern is different, the interactions among the scalars do not change from the ordinal pNGB dark matter model due to $v_s \in \mathbb{R}$ [4]. However, in the light mediator case ($m_{h_2} < m_\chi$), we will show that non-zero elastic cross section with nuclei is induced and can be tested by the current and future direct detection experiments.

In particular, we focus on the mediator mass range of $20 \text{ MeV} \lesssim m_{h_2} \lesssim 200 \text{ MeV}$. This is because the lighter mass region has already been ruled out by the constraint of big bang nucleosynthesis (BBN) [13] while the heavier mass region is insensitive to dark matter direct detection as will be seen below. In the mass range we focus on, the mixing angle $\sin \theta$ is roughly constrained in the range of $2 \times 10^{-5} \lesssim \sin \theta \lesssim 10^{-4}$ [14]. The upper and lower bounds come from the constraints of the meson decays and BBN, respectively.

3 The constraints

Before proceeding to the main subject, we review the constraints relevant to our dark matter scenario.

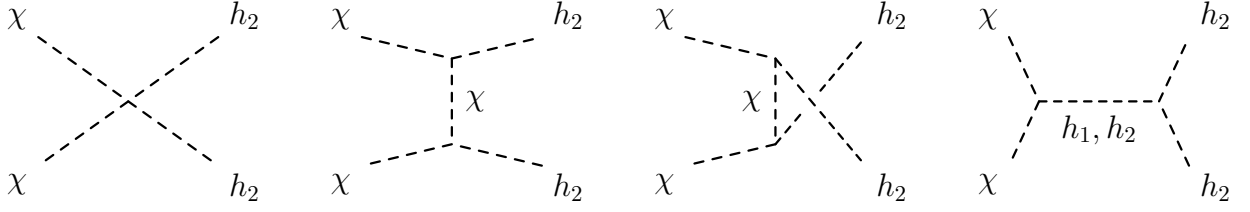


Figure 1: Diagrams for the main dark matter annihilation $\chi\chi \rightarrow h_2h_2$.

3.1 Relic abundance

In the current scenario, the dark matter annihilation channel $\chi\chi \rightarrow h_2h_2$ is dominant in the most of the parameter space. The cross section is calculated from the four diagrams shown in Fig. 1 as

$$\sigma_{h_2h_2}v_{\text{rel}} \approx \frac{\lambda_S^2}{16\pi s} \left| 1 + \frac{m_{h_1}^2}{m_{h_2}^2} \frac{\sin^2 \theta s}{s - m_{h_1}^2 + im_{h_1}\Gamma_{h_1}} \right|^2, \quad (3.1)$$

where s denotes the Mandelstam variable. In the above, $\sin \theta \ll 1$, $m_{h_2} \ll m_{h_1}, m_\chi$ and $m_{h_2}^2 \approx \lambda_S v_s^2$ are used to simplify the equation.

For additional channels $\chi\chi \rightarrow WW, ZZ, f\bar{f}$, the cross sections are calculated as

$$\sigma_{WW}v_{\text{rel}} \approx \frac{\lambda_S g_2^2 m_W^2}{8\pi} \sqrt{1 - \frac{4m_W^2 \sin^2 \theta}{s sm_{h_2}^2}} \left[3 - \frac{s}{m_W^2} + \frac{s^2}{4m_W^4} \right] \frac{m_{h_1}^4}{(s - m_{h_1}^2)^2 + m_{h_1}^2 \Gamma_{h_1}^2}, \quad (3.2)$$

$$\sigma_{ZZ}v_{\text{rel}} \approx \frac{\lambda_S g_2^2 m_Z^2}{16\pi \cos^2 \theta_W} \sqrt{1 - \frac{4m_Z^2 \sin^2 \theta}{s sm_{h_2}^2}} \left[3 - \frac{s}{m_Z^2} + \frac{s^2}{4m_Z^4} \right] \frac{m_{h_1}^4}{(s - m_{h_1}^2)^2 + m_{h_1}^2 \Gamma_{h_1}^2}, \quad (3.3)$$

$$\sigma_{f\bar{f}}v_{\text{rel}} \approx \frac{\lambda_S g_2^2 m_f^2}{32\pi} \left(1 - \frac{4m_f^2}{s} \right)^{3/2} \frac{\sin^2 \theta}{m_W^2 m_{h_2}^2} \frac{m_{h_1}^4}{(s - m_{h_1}^2)^2 + m_{h_1}^2 \Gamma_{h_1}^2}, \quad (3.4)$$

where g_2 is the gauge coupling of the $SU(2)_L$ in the SM and $f\bar{f}$ represents a pair of the SM fermions. Although the other channels $\chi\chi \rightarrow h_1h_1, h_1h_2$ are also possible, the expressions are complicated and not shown here. The full expressions of the annihilation cross sections are given in Appendix A. Note that all the cross sections except for the main channel $\chi\chi \rightarrow h_2h_2$ are suppressed by the small mixing angle $\sin^2 \theta$. Thus it can be seen that the channel $\chi\chi \rightarrow h_2h_2$ tends to be dominant. The annihilation cross section for $\chi\chi \rightarrow h_2h_2$ in Eq. (3.1) is proportional to λ_S^2 while those for the other channels in Eqs. (3.2)–(3.4) are proportional to λ_S .

Then, the thermal averaged cross section can be given by [15]

$$\langle \sigma v_{\text{rel}} \rangle = \frac{1}{16m_\chi^4 T K_2^2(m_\chi/T)} \int_{4m_\chi^2}^{\infty} (\sigma v_{\text{rel}}) \sqrt{s - 4m_\chi^2} s K_1 \left(\frac{\sqrt{s}}{T} \right) ds, \quad (3.5)$$

where T is the temperature of the universe and $K_n(z)$ ($n = 1, 2$) denotes the second kind modified Bessel function. The Boltzmann equation is numerically solved by micrOMEGAs [16] with the above analytic formulas for the annihilation cross sections, and the relic abundance should accommodate the PLANCK observation $\Omega_\chi h^2 \approx 0.12$ [17].¹ Note that the early kinetic decoupling effect may change the parameter space which can reproduce the observed relic abundance when the dark matter mass is close to the SM-like Higgs resonance [19].

3.2 Indirect detection

The main annihilation channel $\chi\chi \rightarrow h_2 h_2$ generates cosmic rays in the galaxy via subsequent h_2 decays. In the mass range we focus on ($30 \text{ MeV} \lesssim m_{h_2} \lesssim 200 \text{ MeV}$), the main decay channel is $h_2 \rightarrow e^+ e^-$, which is constrained by the $e^+ e^-$ observation of AMS-02 [20]. In addition to the $e^+ e^-$ flux, gamma rays are also generated via final state radiation from the produced $e^+ e^-$ and bounded by the observations from dwarf spheroidal galaxies at Fermi-LAT [21]. However this constraint is weaker than the $e^+ e^-$ production [22].² The Cosmic Microwave Background (CMB) may also be distorted by the dark matter annihilation because the produced charged particles and gamma rays ionize the universe after the recombination era. Thus the CMB measurement by PLANCK also sets a bound on the model.

We adopt the model independent bounds for multi-step cascade decays derived in the literature [22] (top left panel in Fig. 11 therein). The extracted bounds are shown in Fig. 2. As can be seen, the AMS-02 bound is severe for $m_\chi \lesssim 100 \text{ GeV}$. For $m_\chi \gtrsim 300 \text{ GeV}$, the CMB bound can be stronger than the AMS-02 bound. However the bound requires $\langle \sigma v_{\text{rel}} \rangle \lesssim \mathcal{O}(10^{-25}) \text{ cm}^3/\text{s}$, which is consistent with thermal relic abundance.

Another comment is that the light mediator h_2 does not induce a long range interaction. Thus we do not need to care about the non-perturbative Sommerfeld effects for the dark matter annihilation [23–27]. This is due to the nature of the pNGB dark matter that all the interactions are written by the derivatives couplings.

¹In the analytic calculations of the cross sections, a large cancellation between the corresponding diagrams occurs due to smallness of v_s . This causes huge numerical errors if the cross sections are automatically evaluated by using public codes such as CalcHEP [18]. Thus the above analytic results are used to evaluate the thermal relic abundance of dark matter in micrOMEGAs [16].

²The other annihilation channels into the SM particles also produce gamma rays. However the constraint is weaker than that of $e^+ e^-$ due to the small cross sections.

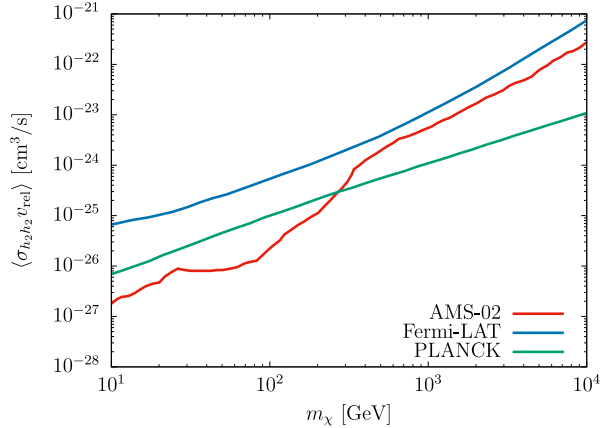


Figure 2: Bounds on the annihilation cross section for $\chi\chi \rightarrow h_2 h_2$ from indirect detection extracted from the literature [22].

3.3 Higgs decay

Since the mediator h_2 is light enough, the SM-like Higgs boson h_1 decays into $h_2 h_2$ whose decay width is calculated as

$$\Gamma_{h_1 \rightarrow h_2 h_2} = \frac{\kappa_{122}^2}{32\pi m_{h_1}} \sqrt{1 - 4 \frac{m_{h_2}^2}{m_{h_1}^2}} \approx \frac{\lambda_S m_{h_1}^3 \sin^2 \theta}{32\pi m_{h_2}^2}, \quad (3.6)$$

where $\sin \theta \ll 1$ and $m_{h_2} \ll m_{h_1}$ are assumed and $m_{h_2}^2 \approx \lambda_S v_s^2$ is used. This decay channel can be regarded as an invisible decay because the lifetime of h_2 is long enough to escape the detector of colliders. In addition to this decay channel, another channel $h_1 \rightarrow \chi\chi$ is also possible if the dark matter mass is $m_\chi < m_{h_1}/2 \approx 62.5$ GeV. The decay width is evaluated as

$$\Gamma_{h_1 \rightarrow \chi\chi} = \frac{m_{h_1}^3 \sin^2 \theta}{32\pi v_s^2} \sqrt{1 - 4 \frac{m_\chi^2}{m_{h_1}^2}} \approx \frac{\lambda_S m_{h_1}^3 \sin^2 \theta}{32\pi m_{h_2}^2} \sqrt{1 - 4 \frac{m_\chi^2}{m_{h_1}^2}}. \quad (3.7)$$

The observation of the Higgs signal strength at the LHC is translated into the constraint of the Higgs invisible decay whose branching fraction should satisfy $\text{Br}_{\text{inv}} \leq 0.11$ [28, 29].

4 Direct detection of pNGB dark matter

It is known that the amplitude for the elastic scattering between the pNGB dark matter and a nucleus $\chi A \rightarrow \chi A$ vanishes in non-relativistic limit of dark matter. This argument is based on the premise that the mass of the mediator h_2 is much heavier than the momentum transfer $q = \sqrt{2m_A E_R}$ [4]. However this is not the case in our scenario where the mass of the mediator h_2 can be the same order or smaller than the momentum

transfer. Assuming $q^2, m_{h_2}^2 \ll m_{h_1}^2$ and $\sin \theta \ll 1$, the differential cross section for the elastic scattering with a nucleus A is calculated as

$$\frac{d\sigma_A}{dE_R} \approx \frac{m_A \kappa_A^2 \sin^2 \theta}{8\pi m_\chi^2 v_\chi^2} \frac{t^2}{v^2 v_s^2 (t - m_{h_2}^2)^2} F^2(E_R), \quad (4.1)$$

where $t = -q^2$ is the Mandelstam variable, v_χ is the velocity of dark matter and $F(E_R)$ is the nuclear Helm form factor which is parametrized by [30]

$$F(E_R) = \frac{3j_1(qR)}{qR} e^{-q^2 \tilde{s}^2 / 2}, \quad (4.2)$$

with the spherical Bessel function $j_1(qR)$, $R \approx \sqrt{r^2 - 5\tilde{s}^2}$ fm, $r \approx 1.2A^{1/3}$ fm, (A is the mass number of the target nucleus) and $\tilde{s} \approx 1$ fm. The Helm form factor is normalized as $F(0) = 1$. The coupling κ_A in Eq. (4.1) is given by

$$\kappa_A = \kappa_p Z + \kappa_n (A - Z) = \sum_q \left[f_q^p m_p Z + f_q^n m_n (A - Z) \right], \quad (4.3)$$

where A and Z are the mass number and the atomic number of the nucleus, respectively. The coefficients f_q^p and f_q^n are the scalar quark form factors of a nucleon, which are chosen as the values in the literature [16]

$$\begin{aligned} f_u^p &= 0.0153, & f_d^p &= 0.0191, & f_s^p &= 0.0447, \\ f_u^n &= 0.0110, & f_d^n &= 0.0273, & f_s^n &= 0.0447, \end{aligned} \quad (4.4)$$

for the light quarks. The form factors of the heavy quarks can be written in terms of those of the light quarks.

Direct detection experiments provide the limits on the elastic scattering cross section with a proton at zero momentum transfer, and the current strongest limit is given by XENON1T/PandaX-4T experiments [1,2]. Note that this limit cannot directly be applied to the current scenario because one cannot simply take zero momentum transfer limit in the differential cross section in Eq. (4.1) due to a strong dependence on the momentum transfer and light mediator mass. However, the experimental limit can be translated into the limit on the total event rate. Then, it is compared with the predicted event rate at a given parameters in the model.³ The differential event rate is given by

$$\frac{dR}{dE_R} = \frac{\rho_\odot}{m_\chi} N_T \int_{v_\chi > v_{\min}} \frac{d\sigma_A}{dE_R} v_\chi f_\odot(\mathbf{v}_\chi) d^3 v_\chi, \quad (4.5)$$

where $\rho_\odot \approx 0.3$ GeV/cm³ is the local dark matter density, N_T is the number of target nucleus, $f_\odot(\mathbf{v}_\chi)$ is the Maxwell-Boltzmann velocity distribution function at the solar

³A similar approach for direct detection with long range interactions due to a light mediator has been discussed [31].

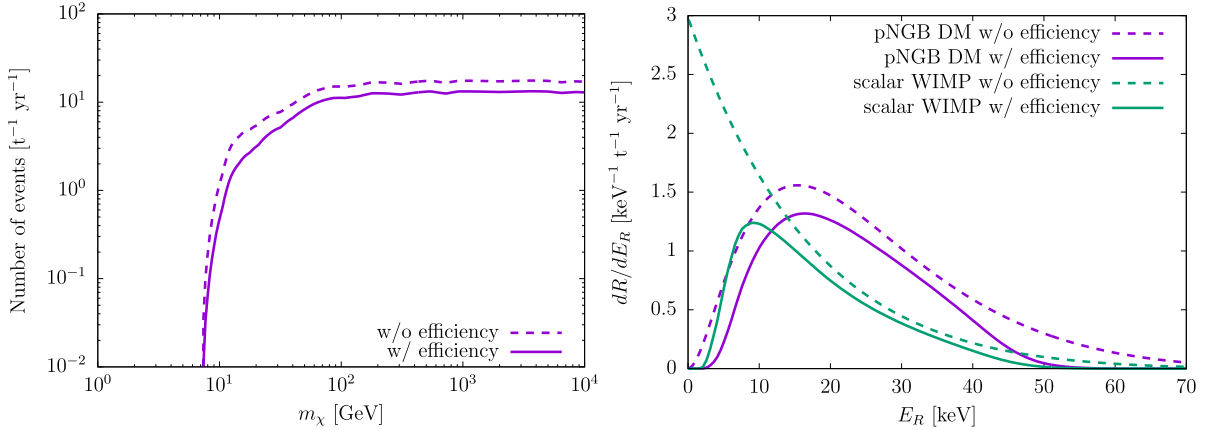


Figure 3: (Left): Limit on the total event rate translated from the XENON1T experiment in the range of the recoil energy $4.9 \text{ keV} < E_R < 40.9 \text{ keV}$ and $1.0 \text{ t} \times \text{yr}$ exposure [1]. The solid (dashed) line represent the limit with (without) the efficiency of the XENON1T detector. (Right): Comparison of energy spectra of number of events for pNGB dark matter and singlet scalar dark matter with $1.0 \text{ t} \times \text{yr}$ exposure where dark matter mass is fixed to be $m_\chi = 150 \text{ GeV}$. The other parameters are taken as $\lambda_S = 0.09$, $\sin \theta = 3 \times 10^{-5}$ and $m_{h_2} = 60 \text{ MeV}$ for the pNGB dark matter, and $\lambda_{hS} = 0.006$ for the singlet scalar dark matter [33]. The solid (dashed) lines represent the spectra with (without) detector efficiency (XENON1T) [1].

system [32], and v_{\min} is the minimum velocity of dark matter at the given recoil energy E_R

$$v_{\min} = \sqrt{\frac{m_A E_R}{2}} \frac{1}{\mu_{A\chi}}, \quad (4.6)$$

where $\mu_{A\chi} = m_A m_\chi / (m_A + m_\chi)$ is the reduced mass between dark matter and nucleus.

For the experimental limit, assuming no isospin violation [34], one can parametrize the differential cross section between dark matter and a nucleus as

$$\frac{d\sigma_A^{\text{exp}}}{dE_R} = \frac{m_A A^2}{2\mu_{p\chi}^2 v_\chi^2} \sigma_p^{\text{exp}} F^2(E_R), \quad (4.7)$$

where σ_p^{exp} is the experimental upper limit on the total elastic cross section with a proton. Using this parametrization, the differential event rate with the experimental limit σ_p^{exp} can be rewritten as

$$\frac{dR^{\text{exp}}}{dE_R} = \frac{\rho_\odot}{m_\chi} N_T \frac{m_A A^2}{2\mu_{p\chi}^2} \sigma_p^{\text{exp}} F^2(E_R) \int_{v_\chi > v_{\min}} \frac{f_\odot(\mathbf{v}_\chi)}{v_\chi} d^3 v_\chi. \quad (4.8)$$

The left panel of Fig. 3 shows the upper bound on the total event rate R^{exp} obtained from the XENON1T limit on the total elastic scattering cross section σ_p^{exp} . The interest

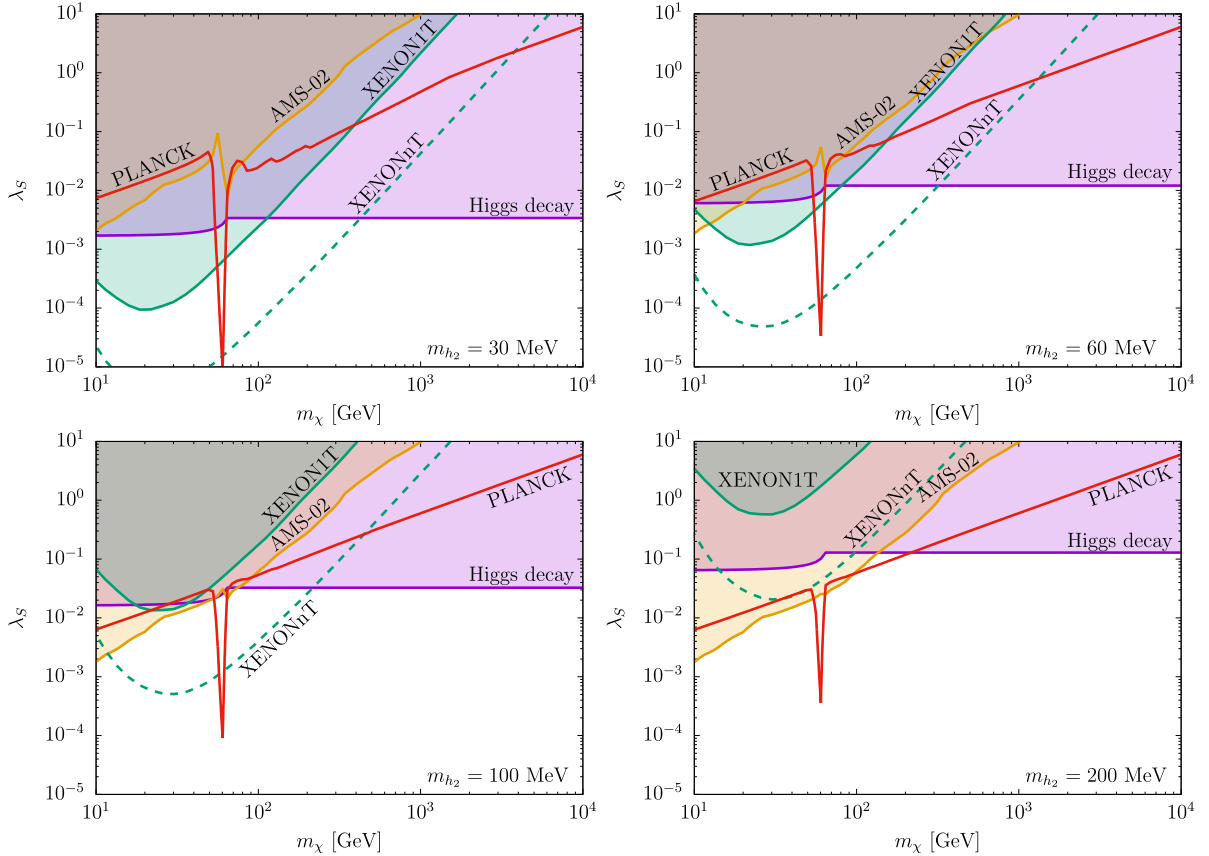


Figure 4: Parameter region in the (m_χ, λ_S) plane for $\sin \theta = 10^{-4}$ and $m_{h_2} = 30, 60, 100$ and 200 MeV. The green, orange and violet region are excluded by XENON1T [1], AMS-02 [20] and Higgs decays [28, 29], respectively. The red line corresponds to the parameter space which can reproduce the observed relic abundance by PLANCK [17].

of region for the recoil energy is $4.9 \text{ keV} < E_R < 40.9 \text{ keV}$ and the exposure $1.0 \text{ t} \times \text{yr}$ is taken into account [1].

The recoil energy spectrum for the pNGB dark matter could be discriminative from the other dark matter candidates thanks to its derivative couplings. The typical energy spectrum for the pNGB dark matter is shown as violet lines in the right panel of Fig. 3. The spectrum for the singlet scalar dark matter (an example of usual WIMPs) is also shown as green lines for comparison [33]. The event rate for the WIMP is enhanced at low energy while that for the pNGB dark matter is suppressed as in the figure. Note that WIMPs may also be able to induce energy spectra similar to the pNGB dark matter if the WIMP mass is heavier and detector efficiency is taken into account because the spectra can have a longer tail at higher energy for heavier WIMPs.⁴ However, the shape of the recoil energy spectrum can be complementarily utilized to discriminate the pNGB dark

⁴Similar spectra may also be induced from the other dark matter scenarios such as WIMPs with momentum dependent cross sections and inelastic scattering processes [32].

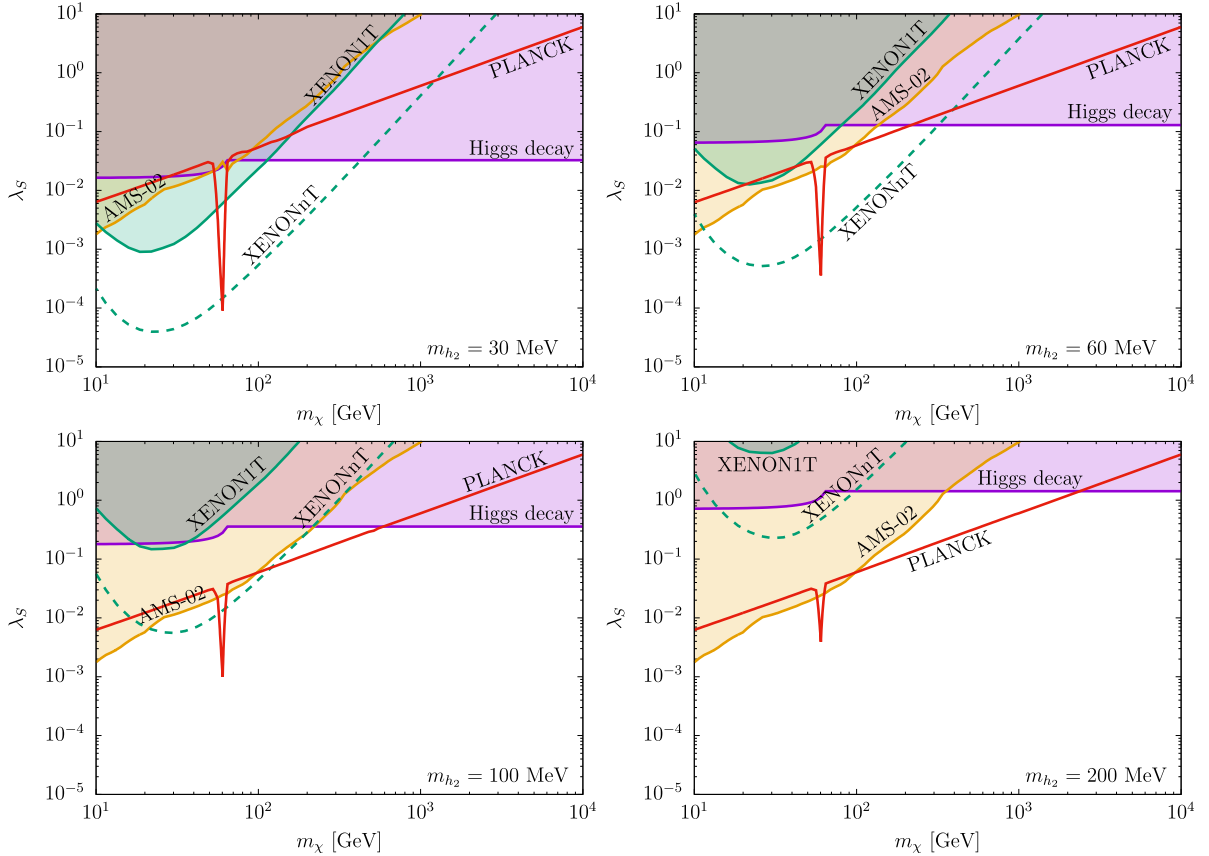


Figure 5: Same plots with Fig. 4 for $\sin \theta = 3 \times 10^{-5}$.

matter and the other candidates combining with the other experiments and observations. Namely, for instance if the dark matter mass is inferred in narrow range by the other experiments or observations, one can use the recoil energy spectrum to discriminate the pNGB dark matter from the usual WIMPs at the end.

Fig. 4 shows the parameter space in the (m_χ, λ_S) plane where the Higgs mixing is fixed to be $\sin \theta = 10^{-4}$ and the second Higgs mass is $m_{h_2} = 30, 60, 100$ and 200 MeV. Fig. 5 shows the same figure with $\sin \theta = 3 \times 10^{-5}$. The green, orange and violet region are excluded by the limit of XENON1T [1], AMS-02 [20] and Higgs decays [28,29], respectively. The green dashed line represents the future sensitivity of the XENONnT experiment [3]. The red line can reproduce the thermal relic abundance consistent with the PLANCK observation $\Omega_\chi h^2 \approx 0.12$ [17]. The constraints of direct detection and Higgs decay tend to be severe for lighter h_2 and larger mixing $\sin \theta$ as can be seen from Eqs. (3.6), (3.7) and (4.1). On the other hand, the AMS-02 bound does not much depend on m_{h_2} except for the region close to the Higgs resonance as obvious from Eq. (3.1). As discussed in Ref. [35], the perturbative unitarity constraint imposes the upper bound on the self quartic coupling as $\lambda_S < 8\pi/3$, however it is invariably weaker than the constraint from Higgs decay in our scenario. From these plots, we can see that the thermally produced pNGB dark matter

with the light mediator can be consistent with all the constraints when the dark matter mass is $m_\chi \sim 100$ GeV for $\sin \theta = 3 \times 10^{-5}$ and $m_{h_2} = 60$ MeV, and can be tested by the future XENONnT experiment.

5 Conclusions

In the previous works, the pNGB dark matter has been completely insensitive to dark matter direct detection experiments because the amplitude for the elastic scattering vanishes in non-relativistic limit. In this paper, we have focused on the case that the particle mediating the elastic scattering is light enough, and we have found that a non-zero contribution to the amplitude emerges. Together with the relevant constraints such as the thermal relic abundance, e^+e^- , gamma ray, CMB and Higgs decays, we have shown the parameter region of this scenario. Some parameter region have already been excluded by the current XENON1T experiment and some other region can be tested by the future XENONnT experiment. The pNGB dark matter can be discriminative from the other dark matter candidates due to complementary study of dark matter direct detection and cosmic ray observations.

Acknowledgements

This work was supported by JSPS Grant-in-Aid for Scientific Research KAKENHI Grant Nos. JP20J11901 (Y.A.), JP20K22349 (T.T.). Numerical computation in this work was carried out at the Yukawa Institute Computer Facility.

A Annihilation cross sections

In this Appendix, we give analytic expressions for all the annihilation channels for completeness. The annihilation cross sections for $\chi\chi \rightarrow h_i h_j$ are given by

$$\begin{aligned} \sigma_{h_1 h_1} v_{\text{rel}} &= \frac{1}{4\pi s} \left(|a_{11}|^2 + \frac{2 \sin^4 \theta m_{h_1}^8}{v_s^4 c_{11}^+ c_{11}^-} \right) \sqrt{1 - \frac{4m_{h_1}^2}{s}} \\ &\quad + \frac{\sin^2 \theta m_{h_1}^4}{4\pi s^{3/2} v_s^2 \sqrt{s - 4m_\chi^2}} \left(2 \text{Re}(a_{11}) + \frac{\sin^2 \theta}{v_s^2} \frac{m_{h_1}^4}{s - 2m_{h_1}^2} \right) \log \left(\frac{c_{11}^+}{c_{11}^-} \right), \end{aligned} \quad (\text{A.1})$$

$$\begin{aligned} \sigma_{h_1 h_2} v_{\text{rel}} &= \frac{1}{2\pi s} \left(|a_{12}|^2 + \frac{2 \sin^2 \theta \cos^2 \theta m_{h_1}^4 m_{h_2}^4}{v_s^4 c_{12}^+ c_{12}^-} \right) \frac{\sqrt{\lambda(s, m_{h_1}^2, m_{h_2}^2)}}{s} \\ &\quad + \frac{\sin \theta \cos \theta m_{h_1}^2 m_{h_2}^2}{2\pi s^{3/2} v_s^2 \sqrt{s - 4m_\chi^2}} \left(2 \text{Re}(a_{12}) + \frac{\sin \theta \cos \theta}{v_s^2} \frac{m_{h_1}^2 m_{h_2}^2}{s - m_{h_1}^2 - m_{h_2}^2} \right) \log \left(\frac{c_{12}^+}{c_{12}^-} \right), \end{aligned} \quad (\text{A.2})$$

$$\begin{aligned} \sigma_{h_2 h_2} v_{\text{rel}} &= \frac{1}{4\pi s} \left(|a_{22}|^2 + \frac{2 \cos^4 \theta m_{h_2}^8}{v_s^4 c_{22}^+ c_{22}^-} \right) \sqrt{1 - \frac{4m_{h_2}^2}{s}} \\ &+ \frac{\cos^2 \theta m_{h_2}^4}{4\pi s^{3/2} v_s^2 \sqrt{s - 4m_{h_2}^2}} \left(2 \operatorname{Re}(a_{22}) + \frac{\cos^2 \theta}{v_s^2} \frac{m_{h_2}^4}{s - 2m_{h_2}^2} \right) \log \left(\frac{c_{22}^+}{c_{22}^-} \right), \end{aligned} \quad (\text{A.3})$$

where s is the Mandelstam variable, the coefficients a_{ij} and c_{ij}^\pm are given by

$$a_{11} = \frac{\sin^2 \theta}{v_s^2} m_{h_1}^2 + \frac{\sin \theta}{2v_s} \frac{\kappa_{111}s}{s - m_{h_1}^2 + im_{h_1}\Gamma_{h_1}} - \frac{\cos \theta}{2v_s} \frac{\kappa_{112}s}{s - m_{h_2}^2 + im_{h_2}\Gamma_{h_2}}, \quad (\text{A.4})$$

$$a_{12} = \frac{\sin \theta \cos \theta}{v_s^2} \frac{m_{h_1}^2 + m_{h_2}^2}{2} - \frac{\sin \theta}{2v_s} \frac{\kappa_{112}s}{s - m_{h_1}^2 + im_{h_1}\Gamma_{h_1}} + \frac{\cos \theta}{2v_s} \frac{\kappa_{122}s}{s - m_{h_2}^2 + im_{h_2}\Gamma_{h_2}}, \quad (\text{A.5})$$

$$a_{22} = \frac{\cos^2 \theta}{v_s^2} m_{h_2}^2 + \frac{\sin \theta}{2v_s} \frac{\kappa_{122}s}{s - m_{h_1}^2 + im_{h_1}\Gamma_{h_1}} - \frac{\cos \theta}{2v_s} \frac{\kappa_{222}s}{s - m_{h_2}^2 + im_{h_2}\Gamma_{h_2}}, \quad (\text{A.6})$$

$$c_{ij}^\pm = s - m_i^2 - m_j^2 \pm \frac{\sqrt{s - 4m_{h_1}^2} \sqrt{\lambda(s, m_{h_i}^2, m_{h_j}^2)}}{\sqrt{s}}, \quad (\text{A.7})$$

with the kinematic function $\lambda(x, y, z) = x^2 + y^2 + z^2 - 2xy - 2yz - 2zx$ and the cubic couplings κ_{ijk} ($i, j, k = 1, 2$) are given in Eqs. (2.10)–(2.13). Γ_{h_i} denotes the total decay width of h_i .

For the other channels, the annihilation cross sections are given by

$$\sigma_{WW} v_{\text{rel}} = \frac{g_2^2 m_W^2}{8\pi} \sqrt{s - 4m_W^2} \frac{s^{3/2}}{v_s^2} \cos^2 \theta \sin^2 \theta \left[3 - \frac{s}{m_W^2} + \frac{s^2}{4m_W^4} \right] \left| \tilde{G}_{h_1} - \tilde{G}_{h_2} \right|^2, \quad (\text{A.8})$$

$$\sigma_{ZZ} v_{\text{rel}} = \frac{g_2^2 m_Z^2}{16\pi \cos^2 \theta_W} \sqrt{s - 4m_Z^2} \frac{s^{3/2}}{v_s^2} \cos^2 \theta \sin^2 \theta \left[3 - \frac{s}{m_Z^2} + \frac{s^2}{4m_Z^4} \right] \left| \tilde{G}_{h_1} - \tilde{G}_{h_2} \right|^2, \quad (\text{A.9})$$

$$\sigma_{f\bar{f}} v_{\text{rel}} = \frac{m_f^2}{8\pi} \sqrt{s} (s - 4m_f^2)^{3/2} \frac{\cos^2 \theta \sin^2 \theta}{v^2 v_s^2} \left| \tilde{G}_{h_1} - \tilde{G}_{h_2} \right|^2, \quad (\text{A.10})$$

where \tilde{G}_{h_i} denotes the h_i propagator and $\left| \tilde{G}_{h_1} - \tilde{G}_{h_2} \right|^2$ is given by

$$\left| \tilde{G}_{h_1} - \tilde{G}_{h_2} \right|^2 = \left| \frac{1}{s - m_{h_1}^2 + im_{h_1}\Gamma_{h_1}} - \frac{1}{s - m_{h_2}^2 + im_{h_2}\Gamma_{h_2}} \right|^2. \quad (\text{A.11})$$

Since the propagator part can be simplified as

$$\left| \tilde{G}_{h_1} - \tilde{G}_{h_2} \right|^2 \approx \frac{m_{h_1}^4}{s^2} \frac{1}{(s - m_{h_1}^2)^2 + m_{h_1}^2 \Gamma_{h_1}^2}, \quad (\text{A.12})$$

when $\sqrt{s}, m_{h_1} \gg m_{h_2}, \Gamma_{h_1}, \Gamma_{h_2}$, one can verify the above cross sections do not violate the unitarity at $s \rightarrow \infty$.

References

- [1] **XENON** Collaboration, E. Aprile *et al.*, *Dark Matter Search Results from a One Ton-Year Exposure of XENON1T*, *Phys. Rev. Lett.* **121** (2018) 111302, [arXiv:1805.12562 \[astro-ph.CO\]](#).
- [2] **PandaX-4T** Collaboration, Y. Meng *et al.*, *Dark Matter Search Results from the PandaX-4T Commissioning Run*, [arXiv:2107.13438 \[hep-ex\]](#).
- [3] **XENON** Collaboration, E. Aprile *et al.*, *Projected WIMP sensitivity of the XENONnT dark matter experiment*, *JCAP* **11** (2020) 031, [arXiv:2007.08796 \[physics.ins-det\]](#).
- [4] C. Gross, O. Lebedev, and T. Toma, *Cancellation Mechanism for Dark-Matter–Nucleon Interaction*, *Phys. Rev. Lett.* **119** (2017) 191801, [arXiv:1708.02253 \[hep-ph\]](#).
- [5] D. Azevedo, M. Duch, B. Grzadkowski, D. Huang, M. Iglicki, and R. Santos, *One-loop contribution to dark-matter-nucleon scattering in the pseudo-scalar dark matter model*, *JHEP* **01** (2019) 138, [arXiv:1810.06105 \[hep-ph\]](#).
- [6] K. Ishiwata and T. Toma, *Probing pseudo Nambu-Goldstone boson dark matter at loop level*, *JHEP* **12** (2018) 089, [arXiv:1810.08139 \[hep-ph\]](#).
- [7] S. Glaus, M. Mühlleitner, J. Müller, S. Patel, T. Römer, and R. Santos, *Electroweak Corrections in a Pseudo-Nambu Goldstone Dark Matter Model Revisited*, *JHEP* **12** (2020) 034, [arXiv:2008.12985 \[hep-ph\]](#).
- [8] C. Arina, A. Beniwal, C. Degrande, J. Heisig, and A. Scaffidi, *Global fit of pseudo-Nambu-Goldstone Dark Matter*, *JHEP* **04** (2020) 015, [arXiv:1912.04008 \[hep-ph\]](#).
- [9] Y. Abe, T. Toma, and K. Tsumura, *Pseudo-Nambu-Goldstone dark matter from gauged $U(1)_{B-L}$ symmetry*, *JHEP* **05** (2020) 057, [arXiv:2001.03954 \[hep-ph\]](#).
- [10] N. Okada, D. Raut, and Q. Shafi, *Pseudo-Goldstone dark matter in a gauged $B - L$ extended standard model*, *Phys. Rev. D* **103** (2021) 055024, [arXiv:2001.05910 \[hep-ph\]](#).
- [11] Y. Abe, T. Toma, K. Tsumura, and N. Yamatsu, *Pseudo-Nambu-Goldstone dark matter model inspired by grand unification*, *Phys. Rev. D* **104** (2021) 035011, [arXiv:2104.13523 \[hep-ph\]](#).
- [12] N. Okada, D. Raut, Q. Shafi, and A. Thapa, *Pseudo-Goldstone Dark Matter in $SO(10)$* , [arXiv:2105.03419 \[hep-ph\]](#).
- [13] A. Fradette and M. Pospelov, *BBN for the LHC: constraints on lifetimes of the Higgs portal scalars*, *Phys. Rev. D* **96** (2017) 075033, [arXiv:1706.01920 \[hep-ph\]](#).

- [14] M. W. Winkler, *Decay and detection of a light scalar boson mixing with the Higgs boson*, *Phys. Rev. D* **99** (2019) 015018, [arXiv:1809.01876 \[hep-ph\]](#).
- [15] P. Gondolo and G. Gelmini, *Cosmic abundances of stable particles: Improved analysis*, *Nucl. Phys. B* **360** (1991) 145–179.
- [16] G. Bélanger, F. Boudjema, A. Goudelis, A. Pukhov, and B. Zaldivar, *micrOMEGAs5.0 : Freeze-in*, *Comput. Phys. Commun.* **231** (2018) 173–186, [arXiv:1801.03509 \[hep-ph\]](#).
- [17] **Planck** Collaboration, N. Aghanim *et al.*, *Planck 2018 results. VI. Cosmological parameters*, *Astron. Astrophys.* **641** (2020) A6, [arXiv:1807.06209 \[astro-ph.CO\]](#). [Erratum: *Astron. Astrophys.* 652, C4 (2021)].
- [18] A. Belyaev, N. D. Christensen, and A. Pukhov, *CalcHEP 3.4 for collider physics within and beyond the Standard Model*, *Comput. Phys. Commun.* **184** (2013) 1729–1769, [arXiv:1207.6082 \[hep-ph\]](#).
- [19] T. Abe, *Early kinetic decoupling and a pseudo-Nambu-Goldstone dark matter model*, [arXiv:2106.01956 \[hep-ph\]](#).
- [20] **AMS** Collaboration, L. Accardo *et al.*, *High Statistics Measurement of the Positron Fraction in Primary Cosmic Rays of 0.5–500 GeV with the Alpha Magnetic Spectrometer on the International Space Station*, *Phys. Rev. Lett.* **113** (2014) 121101.
- [21] **Fermi-LAT, DES** Collaboration, A. Albert *et al.*, *Searching for Dark Matter Annihilation in Recently Discovered Milky Way Satellites with Fermi-LAT*, *Astrophys. J.* **834** (2017) 110, [arXiv:1611.03184 \[astro-ph.HE\]](#).
- [22] G. Elor, N. L. Rodd, T. R. Slatyer, and W. Xue, *Model-Independent Indirect Detection Constraints on Hidden Sector Dark Matter*, *JCAP* **06** (2016) 024, [arXiv:1511.08787 \[hep-ph\]](#).
- [23] J. Hisano, S. Matsumoto, and M. M. Nojiri, *Unitarity and higher order corrections in neutralino dark matter annihilation into two photons*, *Phys. Rev. D* **67** (2003) 075014, [arXiv:hep-ph/0212022](#).
- [24] J. Hisano, S. Matsumoto, and M. M. Nojiri, *Explosive dark matter annihilation*, *Phys. Rev. Lett.* **92** (2004) 031303, [arXiv:hep-ph/0307216](#).
- [25] J. Hisano, S. Matsumoto, M. M. Nojiri, and O. Saito, *Non-perturbative effect on dark matter annihilation and gamma ray signature from galactic center*, *Phys. Rev. D* **71** (2005) 063528, [arXiv:hep-ph/0412403](#).
- [26] J. Hisano, S. Matsumoto, O. Saito, and M. Senami, *Heavy wino-like neutralino dark matter annihilation into antiparticles*, *Phys. Rev. D* **73** (2006) 055004, [arXiv:hep-ph/0511118](#).

- [27] J. Hisano, S. Matsumoto, M. Nagai, O. Saito, and M. Senami, *Non-perturbative effect on thermal relic abundance of dark matter*, [Phys. Lett. B **646** \(2007\) 34–38](#), [arXiv:hep-ph/0610249](#).
- [28] **CMS** Collaboration, A. M. Sirunyan *et al.*, *Search for invisible decays of a Higgs boson produced through vector boson fusion in proton-proton collisions at $\sqrt{s} = 13$ TeV*, [Phys. Lett. B **793** \(2019\) 520–551](#), [arXiv:1809.05937 \[hep-ex\]](#).
- [29] **ATLAS** Collaboration, M. Aaboud *et al.*, *Combination of searches for invisible Higgs boson decays with the ATLAS experiment*, [Phys. Rev. Lett. **122** \(2019\) 231801](#), [arXiv:1904.05105 \[hep-ex\]](#).
- [30] J. D. Lewin and P. F. Smith, *Review of mathematics, numerical factors, and corrections for dark matter experiments based on elastic nuclear recoil*, [Astropart. Phys. **6** \(1996\) 87–112](#).
- [31] T. Hambye, M. H. G. Tytgat, J. Vandecasteele, and L. Vanderheyden, *Dark matter direct detection is testing freeze-in*, [Phys. Rev. D **98** \(2018\) 075017](#), [arXiv:1807.05022 \[hep-ph\]](#).
- [32] C. McCabe, *The Astrophysical Uncertainties Of Dark Matter Direct Detection Experiments*, [Phys. Rev. D **82** \(2010\) 023530](#), [arXiv:1005.0579 \[hep-ph\]](#).
- [33] **GAMBIT** Collaboration, P. Athron *et al.*, *Status of the scalar singlet dark matter model*, [Eur. Phys. J. C **77** \(2017\) 568](#), [arXiv:1705.07931 \[hep-ph\]](#).
- [34] J. L. Feng, J. Kumar, D. Marfatia, and D. Sanford, *Isospin-Violating Dark Matter*, [Phys. Lett. B **703** \(2011\) 124–127](#), [arXiv:1102.4331 \[hep-ph\]](#).
- [35] C.-Y. Chen, S. Dawson, and I. M. Lewis, *Exploring resonant di-Higgs boson production in the Higgs singlet model*, [Phys. Rev. D **91** \(2015\) 035015](#), [arXiv:1410.5488 \[hep-ph\]](#).